

FULL ARTICLE

Comparison of dermal vs internal light administration in human lungs using the TDLAS-GASMAS technique—Phantom studies

Jim Larsson^{1*}  | Dennis Leander² | Märta Lewander Xu² | Vineta Fellman³ | Joakim Bood¹ | Emilie Krite Svanberg^{4,5}

¹Division of Combustion Physics, Department of Physics, Lund University, Lund, Sweden

²GPX Medical AB, Lund, Sweden

³Department of Clinical Sciences, Lund, Pediatrics, Lund University and Division of Neonatology, Skåne University Hospital, Lund, Sweden

⁴Department of Physics, Lund Laser Centre, Lund University, Lund, Sweden

⁵Department of Clinical Sciences, Anesthesiology and Intensive Care Medicine, Skåne University Hospital, Lund University, Lund, Sweden

*Correspondence

Jim Larsson, Division of Combustion Physics, Department of Physics, Lund University, Lund, Sweden.
Email: jim.larsson@forbrf.lth.se

Funding information

Departments of Pediatrics and Physics, Lund University; Eurostars, Grant/Award Number: E! 9833 Neo-Lung; Laserlab-europe, Grant/Award Number: EUH2020 654148

Abstract

Oxygen and water vapor content, in the lungs of a 3D-printed phantom model based on CT-images of a preterm infant, is evaluated using Tunable Diode Laser Absorption Spectroscopy (TDLAS) in Gas in Scattering Media Absorption Spectroscopy (GASMAS), that is, the TDLAS-GASMAS technique. Oxygen gas is detected through an absorption line near 764 nm and water vapor through an absorption line near 820 nm. A model with a



lung containing interior structure is compared to a model with a hollow lung. Compared to the model with the hollow lung, both the mean absorption path length and the transmitted intensity are found to be lower for the model with the structured lung. A new approach, where laser light is delivered internally into the model through an optical fiber, is compared to dermal light administration, that is, illumination onto the skin, for the model with structure inside the lung. The internal light administration generally resulted in larger gas absorption, and higher signal-to-noise ratios, compared to the dermal light administration. The results from the phantom measurements show great promise for the internal illumination approach and a natural next step would be to investigate it further in clinical studies.

KEYWORDS

3D-print, GASMAS, light scattering, optical phantom, oxygen evaluation, preterm infant, TDLAS

1 | INTRODUCTION

Preterm born infants have major morbidities related to organ immaturity. Lung immaturity is characterized by paucity of alveoli with decreased amount of lipoprotein surfactant resulting in variations in the aeration of the lung tissue. Despite modern surfactant replacement therapy, the disrupted pulmonary vascularization, inflammation, and

treatment injury in the immature lung lead to long-term lung morbidity, that is, bronchopulmonary dysplasia [1]. With the increasing survival rate in extremely preterm born (born before 28 weeks of gestation), the number of infants with neonatal pulmonary disorder is increasing [2] and subsequently the number of children with decreased lung function at school age [3]. Thus, there is an urgent need to improve the treatment and diagnostic methods of neonatal pulmonary

diseases in preterm infants. The current golden standard for diagnosis, assessments of lung aeration, complications and treatment evaluation, is pulmonary X-ray investigations. However, frequent exposure to radiation is harmful for small infants under development and carries a substantially increased risk of later development of malignancies [4, 5]. Furthermore, X-ray imaging only provides occasional “snapshot” views of the lungs. Especially assessing the efficacy of mechanical ventilation, a noninvasive lung monitoring device would be a very attractive scenario.

Research efforts have been directed towards development of noninvasive alternatives to X-ray imaging. Electrical impedance tomography [6, 7] is a noninvasive technique, currently on a research level, providing information on global and regional changes in lung impedance, correlating with intrathoracic changes in air content and lung volume. However, this technique, even on a research level, only provides information on a transversal “slice” of the lung and does not provide any information on regional oxygen content. Another noninvasive diagnostic technique is lung ultrasound imaging [8], which is a modality that is frequently used in the intensive care units to detect pneumothorax (collapsed lung), consolidated lung parts and pleural effusions (eg, blood). However, ultrasound is not able to penetrate into the lung since nearly 100% of the ultrasound pulses are reflected by gas, and therefore no information about the oxygen concentration/amount of air in the lungs can be obtained. Ultrasound is also a highly user-dependent modality and will only provide momentary information.

Recently, possibilities are starting to arise within the field of noninvasive spectroscopic pulmonary oxygen measurements with the laser-based technology TDLAS (Tunable Diode Laser Absorption Spectroscopy)-GASMAS (Gas in Scattering Media Absorption Spectroscopy), with a pilot study [9] showing that detection of oxygen gas was possible in a group of 29 studied newborn infants, using optical spectroscopy applied noninvasively on the thoracic skin.

The GASMAS technique [10] is based on TDLAS, that is, narrow-band diode laser absorption spectroscopy, but applied to the situation when the absorbing free gas is dispersed in pores and cavities inside a surrounding medium, typically heavily light scattering (such as human tissue). The surrounding medium exhibits absorption features orders of magnitudes broader than those of the gas, making the gas detectable despite heavy background absorption. Therefore, we anticipate that the TDLAS-GASMAS method could potentially be used to monitor changes in oxygen content in the lungs of preterm infants. Immediately after birth the fluid in the lungs will be replaced by air. This transaction should be detectable. In healthy lungs, the oxygen concentration varies between 14% and 21% [11], with fluctuation in relation to the breathing phase (inhalation or exhalation). In atelectasis

(partial closure of the lung) with decreased lung volume and oxygen content, the method should show a decrease in oxygen absorption and transmission in that particular area. In pneumothorax on the other hand, the air-filled pleural cavity is expected to result in higher oxygen absorption.

A particular challenge is to define the optimal positioning of the light injection and detection probes as the light travels through scattering tissue on its way to the gas inside the lungs and then on its way to the detector. In order to better understand the geometrical considerations for TDLAS-GASMAS measurements, we have performed a study on a 3D-printed thoracic phantom, simulating real conditions in newborn infants [12, 13], giving much insight into the diffuse light propagation through the tissue. In the previous studies, the light illumination and detection have been performed dermally, that is, with the laser source and detector applied onto the skin. However, the heavy attenuation due to the strong light scattering and absorption in human tissue strongly limits the amount of light that reaches the lung volume and thereafter the detector, resulting in very faint gas signals.

These observations led to the insight that much could be gained by instead supplying the light internally using an optical fiber inserted into a clinically needed nasogastric or endotracheal tube (ie, a noninvasive approach without penetrating the tissue of the infant), while still performing the detection dermally [14–16]. By administering the light internally, much more light is expected to be detected since the exponential light attenuation is strongly influenced by substantially reducing the optical path length through the surrounding tissue, while ensuring that basically all detected photons have passed through the gas-filled lung tissue. A standard clinical application where a nasogastric tube is used also for monitoring is Neurally Adjusted Ventilatory Assist (NAVA). In such an application, the nasogastric tube contains an array of electrodes collecting the electromyographic signal from the diaphragm thereby assisting in patient synchronization with the ventilator, and preventing the main breathing muscle from atrophy [17].

In this study, we aim to investigate the technical benefits of internal light administration. We present GASMAS measurements on a new thoracic phantom, where gas signals obtained using a novel internal distribution geometry are compared to those obtained for dermal light administration. Oxygen gas is detected through an absorption line near 764 nm and water vapor through an absorption line near 820 nm. The mean absorption path length can be estimated from the measured water absorption at 820 nm, since the water concentration can be estimated from the vapor pressure at the prevailing temperature. Then, assuming that the mean absorption path length is the same at 764 and 820 nm, the oxygen concentration can be determined from the measured oxygen absorption at 764 nm. In the following section,

we describe the experimental setup and the tissue phantom. In Section 3 the results are presented and discussed, before the paper ends with conclusions in Section 4.

2 | METHODS

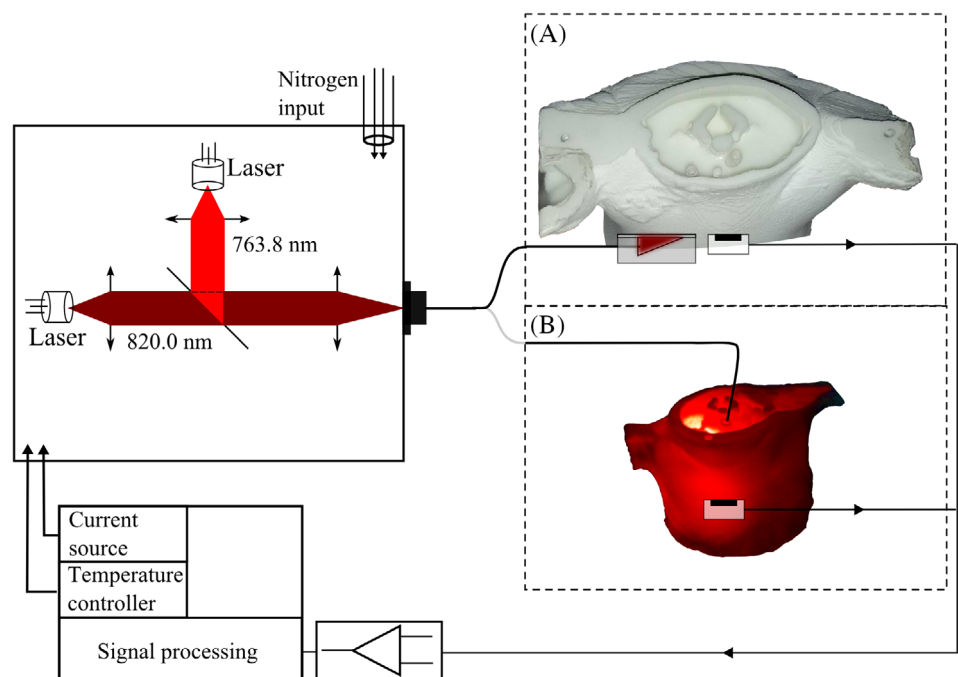
2.1 | Experimental setup

The system used in this study was developed within the EU-financed Eurostar project Neo-Lung [18] by the company GPX Medical, with the aim to develop a first prototype system for larger clinical validations. Four different partners: GPX Medical AB (Sweden), Nanoplus Nanosystems and Technologies GmbH (Germany), Lund University (Sweden), and Norsk Elektro Optikk AS (Norway) are collaborating in evaluating and developing the technology. The experimental setup is schematically depicted in Figure 1. Two diode lasers emitting light with wavelengths centered at 763.8 nm (22.1 mW, DFB laser, Nanoplus, Germany) and 820.0 nm (11.4 mW, DFB laser, Nanoplus, Germany) were time multiplexed and scanned, at a frequency of 1 kHz, over the P9P9 and P9Q8 transitions in the O₂ A-band and the (101 ← 202) transition in H₂O by modulating the injection current using an electronic platform (Laser Gas III, Norsk Elektro Optikk, Norway). The laser light from the two lasers were superimposed using a dichroic mirror and was then coupled into a 400- μ m diameter optical fiber. In order to avoid measuring absorption signals due to ambient air, the diode lasers and the optics were enclosed in a nitrogen filled case.

The fiber-end solution of the optical fiber depended on whether dermal or internal light administration was used.

Both solutions were based on creating diffuse light emission with a maximum irradiance below 150 mW/cm², which exposed on the skin would generate a maximum temperature increase of 2°C [19]. The diffuser was milled from a solid piece of white polytetrafluoroethylene (PTFE), had gold plated reflecting walls, and was filled with silicone to avoid offset absorption signals from ambient air. The other fiber-end solution for internal light administration had hot-melt adhesive and white nylon powder mixture attached to the end of the optical fiber to provide a homogenous illumination around the fiber tip. The transmitted light was collected and detected with a 10 × 10 mm² photodiode (S3590-08, Hamamatsu, Japan). Typical signals from water and oxygen are shown in Figure 2. The signals were intensity normalized and unwanted frequencies were filtered out through an electronic platform (Laser Gas III, Norsk Elektro Optikk, Norway), after which the absorption magnitude was acquired from a proprietary algorithm by Norsk Elektro Optikk. As can be seen in Figure 2, the background is dominated by fringes due to interference phenomena induced by optical components and the sample itself. Although the signal shape is reminiscent of wavelength modulation spectroscopy (WMS), it should be pointed out that WMS was not performed, and the shape is only due to the data processing algorithm used. The processed absorption signal (Figure 2) was calibrated against reference signals recorded at known conditions, where the Beer-Lambert law can be approximated as a linear function, producing an absorption value which is the product of the relative concentration of the absorbing species (%) and the mean absorption path length, L_{Abs} (m).

FIGURE 1 Sketch of the experimental setup. The light from two lasers at 763.8 and 820.0 nm were superimposed and coupled into an optical fiber. For delivering the light into the sample, two fiber end solutions were used. (A) A diffuser to deliver homogenous laser light over a larger area, used for the percutaneous measurements. (B) Fiber probe for invasive measurements, the fiber tip is made diffuse for isotropic illumination of the surrounding tissue



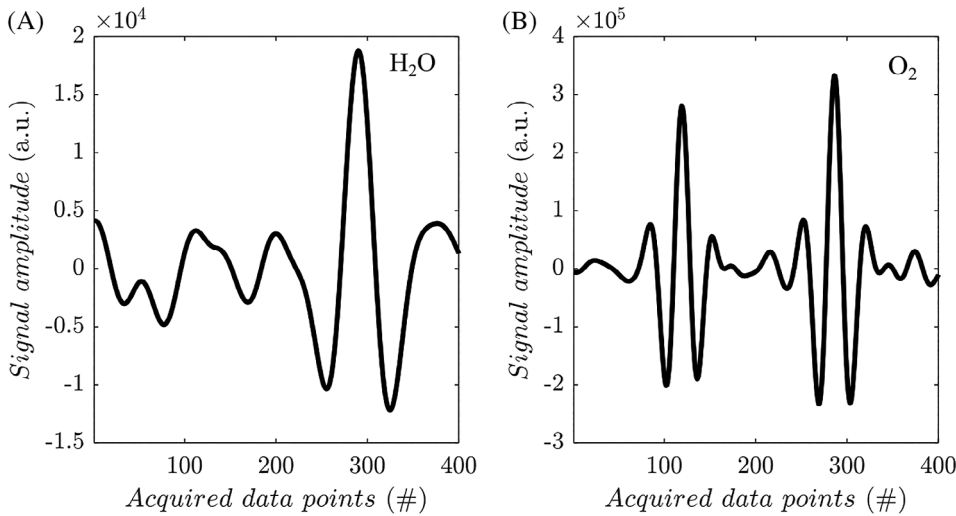


FIGURE 2 Filtered absorption signals from a dermal measurement on the structure lung model of a water vapor absorption peak at 820.0 nm (A) and two absorption peaks of oxygen at 763.8 nm (B). It should be noted that the wavelength scales are based on data points

2.2 | Phantom model

The phantom model was 3D-printed using nylon in four different components which in the computer tomography (CT) images of the torso of a newborn infant had been identified as bone, heart, lungs and a subcutaneous fat layer surrounding the torso. The bone was printed solid and only the boundary layer of the heart, lungs and fat layer were printed. The current 3D-printed phantom model is an improved version, for example, smoother surfaces, of the phantom model used in an earlier study [13]. The hollow organs, excluding the lungs, were filled with a liquid phantom, consisting of a mixture of Indian Ink (Rotring Germany), Intralipid 20% (Fresenius Kabi, Sweden) and water, with optical properties similar to real tissue corresponding to heart, fat and muscle tissue. The optical properties of the liquid phantom were evaluated at 764 and 820 nm using a photon time-of-flight setup [20] with an infinite slab geometry (Table 1).

Two different lung phantoms were used in the present study, one that was hollow, that is, air-filled, and one where absorption and scattering properties were added to the lung volume by filling the lungs with a sponge material. The lung had a total volume of 75 cm³, a maximum height measured to 7 cm and a width of 6 cm. The total dimension of the 3D-printed torso had an approximate size of 10 × 10 × 8 cm and the liquid phantom volumes were divided into 270 cm³ of muscle phantom, 100 cm³ of fat phantom and 35 cm³ of heart phantom.

2.3 | Experimental protocol

As depicted in Figure 3, the dermal measurement geometries were defined as 10 different areas around the torso; four on the front (*F1*, *F2*, *F3*, *F4*), four on the back (*B1*, *B2*, *B3*, *B4*), and under the armpits, *AR* and *AL*. When performing

all-dermal measurements, the light source and detector were positioned on the surface of the printed model. The same measurement positions for the detector were considered also when the light source was placed inside the model, both through the trachea (air pipe) and just posterior in the location to where the human esophagus (food pipe) is positioned. For each source-detector position, the absorption from oxygen, at 763.8 nm, and water vapor, at 820.0 nm, was probed by alternately switching between the two diode lasers. The obtained signals were averaged over 20 seconds and 10 signals were recorded to determine a mean value and SD.

2.4 | Gas concentration evaluation

A challenge when evaluating gas concentrations in porous scattering media using absorption spectroscopy is the unknown absorption path length, yielding two unknown independent parameters in the Beer-Lambert equation, that

TABLE 1 Absorption (μ_a , μ_a') and scattering (μ_s , μ_s') coefficients as measured with time-of-flight spectroscopy for the different phantoms, corresponding to muscle, heart and fat tissue, nylon and the sponge material filling out one of the lung phantoms

	764 nm		820 nm	
	μ_a (cm ⁻¹)	μ_s' (cm ⁻¹)	μ_a (cm ⁻¹)	μ_s' (cm ⁻¹)
Muscle phantom	0.34	7.96	0.31	7.22
Heart phantom	0.38	5.43	0.34	4.77
Fat phantom	0.13	10.14	0.12	9.21
Nylon	0.017	40.07	0.012	36.51
Sponge material (lung phantom)	0.44	3.44	0.47	3.10

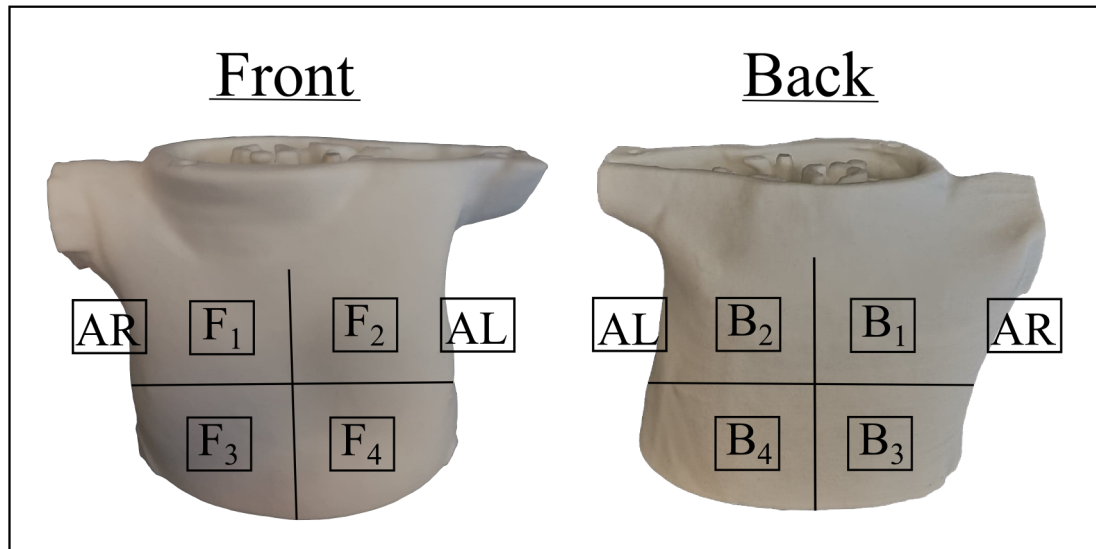


FIGURE 3 Phantom measurement positions considered, divided into four areas on the front (F), four areas on the back (B), and one area under the right armpit (AR) and one under the left armpit (AL)

is, the concentration and the absorption path length, which makes it unsolvable. One method that overcomes this problem is to measure the absorption of a second gas with known concentration and absorption cross section, extract the mean absorption path length from this measurement and then use this value in the Beer-Lambert equation to estimate the unknown concentration. In this experiment, the measurements were performed at atmospheric conditions. The absorption path length reported in the result section was calculated assuming that both the water vapor and oxygen concentrations are known, since these concentrations can be estimated by monitoring the temperature of the phantom and assuming an atmospheric oxygen concentration and a relative humidity of 100% in the lung. As the aim of the technique is to monitor oxygen content, the oxygen concentration was evaluated by equating the absorption path length of water vapor and oxygen. Having the absorption path lengths equal for the gases assumes that the light propagation is equal, which, however, is not entirely true for light of different wavelengths. That is why the weaker absorption band of water vapor at 820 nm was chosen over the stronger absorption band located at 935 nm which has been used in previous studies.

3 | RESULTS AND DISCUSSION

3.1 | Comparing dermal measurements on hollow and structured lungs

Dermal measurements (Figure 1A) were performed on the model with the structured lung. Due to substantial extinction of the light when introducing the structured lung, many of the possible permutations of source-detector positions

(Figure 3) yielded transmitted power below 100 nW, which for the current system was below the limit to obtain a detectable absorption signal. Absorption signals obtained with the structured lung were then compared to the same source-detector positions as for the hollow lung (see Figure 4). For the structured lung, with the detector placed under the right armpit ($D:AR$), absorption signals were obtained for laser source positions (S) F_1 , F_3 and the position between F_1 and F_2 (position $F_{1,2}$ in Figure 4). With the detector positioned under the left armpit ($D:AL$), detectable absorption signals were obtained for source positions F_2 and F_4 . No detectable absorption signals were obtained when the laser source was positioned on the back of the model, due to insufficient amount of transmitted light.

As can be seen in Figure 4, the measurements on the structured lung overall resulted in lower values of both the absorption path length and the detected intensity compared to measurements performed on the hollow lung. However, similar values of the detected intensity were obtained at the source-detector position $S:F_1 D:AR$ for the structured and hollow lung. This might indicate that much of the light that reached the detector only went through the liquid phantom and not the structured lung, which is supported by the short observed absorption path lengths, 2.0 ± 0.15 cm and 2.2 ± 0.13 cm, for H_2O and O_2 , respectively.

3.2 | Internal light administration

The optical fiber, as described in Section 2.1, was inserted into the 3D-printed model with the structured lung at two different locations. For the first measurement position, the optical fiber ends in the trachea of the 3D-printed lung. For the second measurement position, the optical fiber was

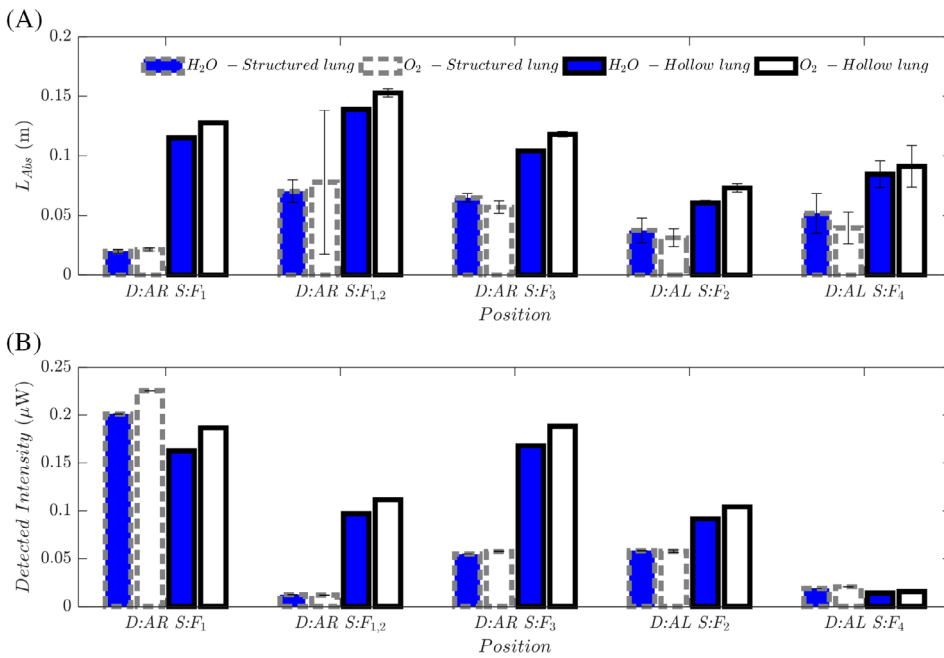


FIGURE 4 Measurements performed on the 3D-printed model having a structured lung (gray-dashed edge line) or a hollow lung (black edge line). The mean absorption path length (A) and the detected intensity (B) for water vapor (H₂O, blue bar) and oxygen (O₂, white bar), were obtained for the detector (D) positioned under the right (AR) and left (AL), and the laser source applied at different positions on the front (F) of the 3D-printed model

inserted into the liquid phantom simulating muscle tissue, ending 4 cm from the top of the model, posterior to the trachea and anterior to the vertebral column. This location corresponds with the anatomical placement of the esophagus.

With the optical fiber inserted into the model, absorption signals were detectable on both the front and back of the model. Mean absorption path length (L_{Abs}) and transmitted laser intensity were measured for both oxygen and water vapor. Detectable signals, for the different detector positions with the light delivered through the trachea, as presented in Figure 5, were observed at the upper part of the model (positions AR, F₁, B₁, B₂ and B₃). The corresponding results

obtained with the light delivered at the other location, that is, corresponding to the location of esophagus, are shown in Figure 6. In this case detectable signals were obtained on the right side, that is, positions AR, F₁, F₃, B₁ and B₃. The absence of a detectable signal on the bottom left side at the back of the model (position B₄) can be attributed to the presence of the heart and the smaller lung volume on the left side of the model.

Measurements using the optical fiber yielded a maximum mean absorption path length of 13.2 ± 1.4 cm and 10.9 ± 0.8 cm for water vapor and oxygen, respectively, with light delivery in the esophagus and detection in position AR. The maximum mean signal-to-noise ratio (SNR) was

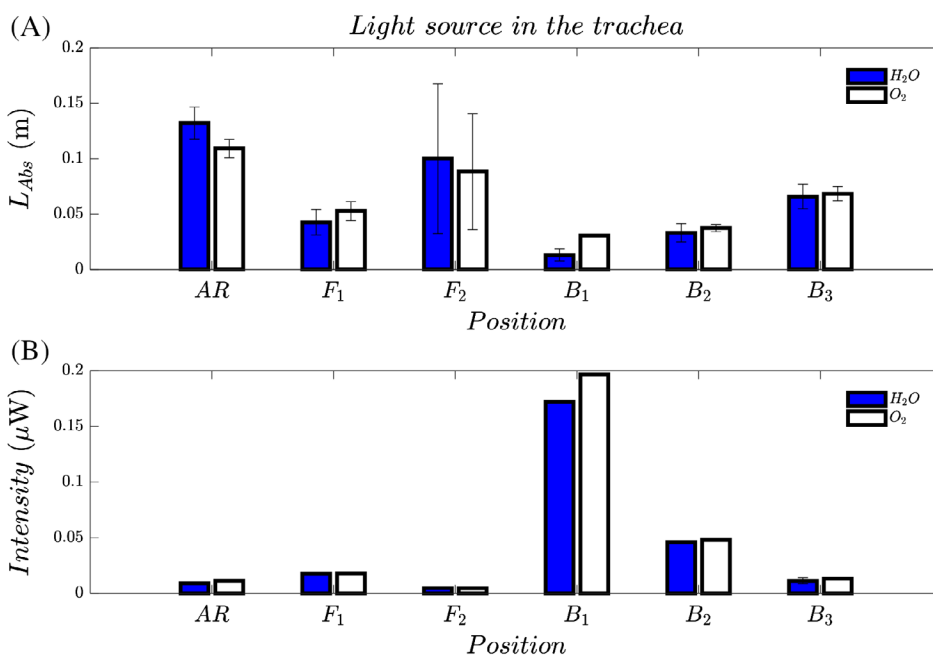
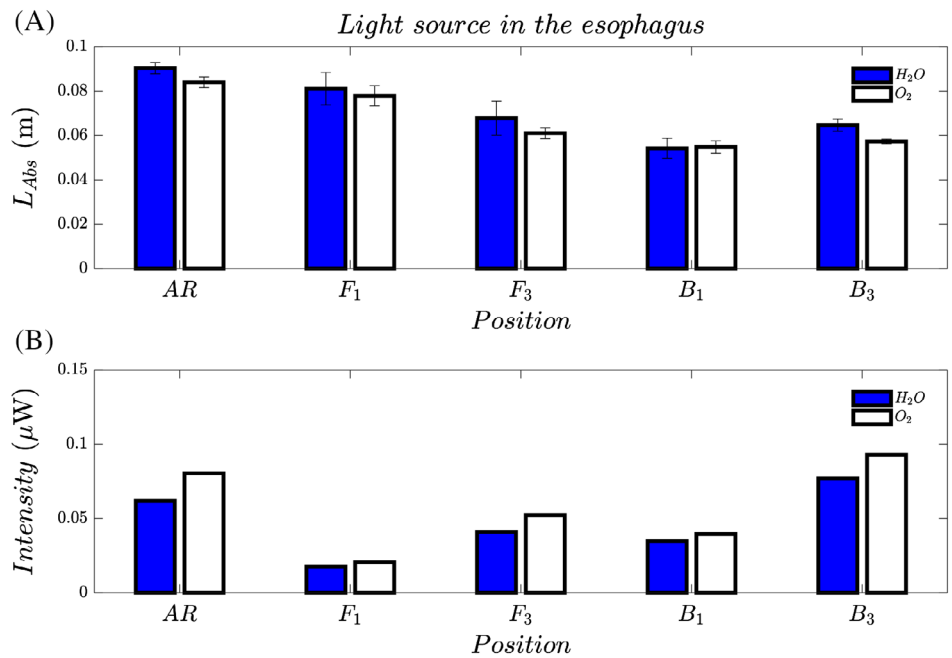


FIGURE 5 Measurements performed with the optical fiber inserted into the trachea of the 3D-printed model with the structured lung. The (A) absorption path length for oxygen (O₂, white bar), water vapor (H₂O, blue bar) and (B) the transmitted intensity, were measured for the detector positions AR (right armpit), F₁ (front), F₂ (front), B₁ (back), B₂ (back), B₃ (back)

FIGURE 6 Measurements performed with the optical fiber inserted in the liquid phantom, of the 3D-printed model, where the esophagus anatomically is located. The (A) absorption path length for oxygen (O_2 , white bar), water vapor (H_2O , blue bar) and (B) the transmitted intensity, were measured for the detector positions AR (right armpit), F1 (front), F3 (front), B1 (back), B2 (back)



obtained for position $B3$ when the source was placed in the esophagus. The obtained mean SNR of 10.4 (H_2O) and 55.7 (O_2) gives, for this position, a detection limit for water vapor at 3.58% and for oxygen 0.1%. The SNR was evaluated by dividing the amplitude of the signal (Figure 2) with the root mean square (rms) of the background signal. It should be noticed that the background signal contains both random noise and interference fringes.

A development goal of the measurement system is to be able to continuously monitor the oxygen concentration by

using the absorption path length obtained from the water vapor signal to calculate the oxygen concentration. Evaluated oxygen concentrations for illumination through trachea and the location corresponding to esophagus are presented in Figure 7A,B, respectively. The oxygen concentration for all measurement positions in the trachea geometry (Figure 7A) was evaluated to $25.9 \pm 11.7\%$ and in esophagus (Figure 7B) to $19.5 \pm 1.0\%$. The large difference in precision between the data obtained for the two fiber positions was attributed to an overall higher detected intensity in the esophagus geometry.

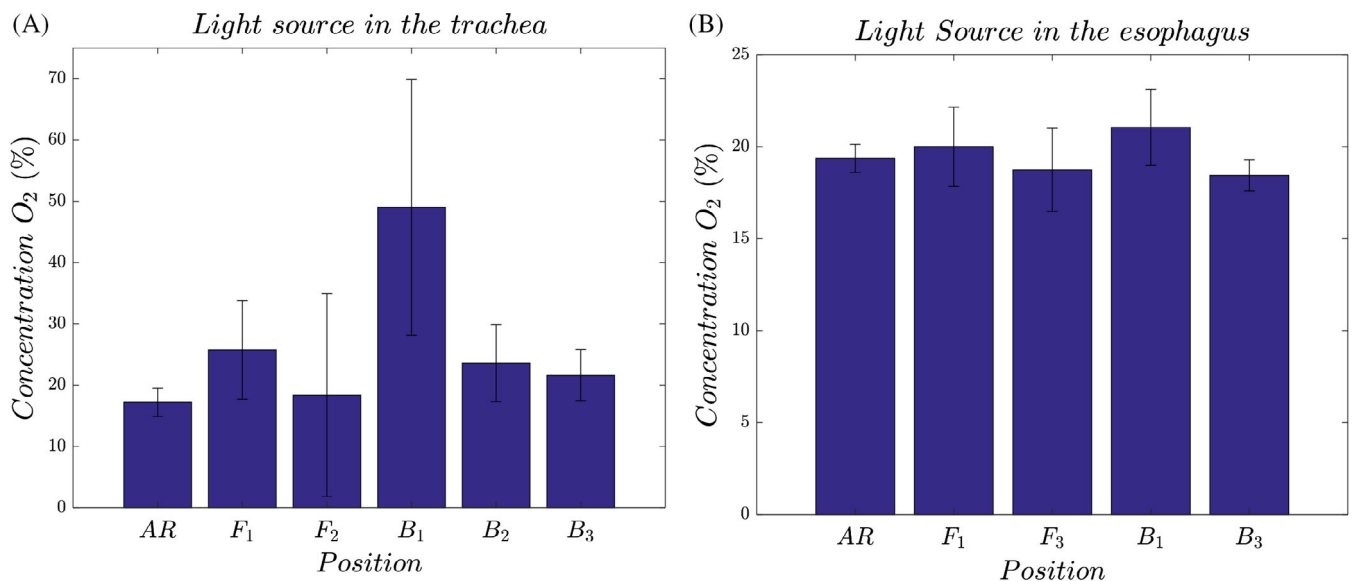


FIGURE 7 Calculated oxygen concentration (O_2) from the absorption obtained from O_2 and H_2O for detector positions AR (right armpit), F1 (front), F2 (front) F3 (front), B1 (back), B2 (back) and B3 (back). The mean absorption path length of water vapor (H_2O) was obtained by knowing the temperature of the phantom and assuming a relative humidity of 100%, and then used to calculate the oxygen concentration from the absorbance of oxygen. This was done for both the (A) tracheal and the (B) esophageal measurements

4 | CONCLUSION

In the current study we observed a generally larger absorption path length for internal light illumination compared to the dermal measurement geometry when measuring on the structured lung model. For the tracheal measurement geometry, the obtained absorption signals show a larger variation between different detector positions compared to the esophagus geometry. A possible explanation could be that the optical fiber in the esophagus geometry is positioned closer to the bottom half of the lung, which carries a larger volume, which suggests that the esophagus geometry would be preferable to more readily obtain absorption signals. The GASMAS technique relies on sufficient transmission of light through tissue in order to obtain an acceptable signal. Thus, higher signal intensities were obtained for the internal light illumination approach as compared to the all-dermal approach, since less tissue was penetrated in the former case. The results also show that the location of the detector is less critical with internal light illumination.

This is the first study presenting results of GASMAS on a lung phantom, mimicking a thoracic cavity utilizing absorption lines of water vapor near 820 nm, instead of the previously used wavelength of 935 nm. This new wavelength selection is advantageous since the scattering and absorption coefficients are more similar to their values at 764 nm, used for oxygen detection. The new choice of nearby wavelengths results in higher measurement accuracy since this better justifies the evaluation procedure assuming the same optical path length in the measurements of the two species. Our results show that the highest accuracy in the measured oxygen concentration is obtained with internal light administration with the fiber end located close to a position corresponding to the location of esophagus, where it is $\pm 1\%$. This accuracy is expected to be high enough to distinguish between healthy and diseased neonates, including preterm neonates.

The GASMAS technique shows great potential to be developed into a continuous patient surveillance technique. As the targeted group of patients for future studies, that is, preterm infants with pulmonary disease, usually needs a nasogastric feeding line it is feasible to administer diffuse laser light through fibers positioned in the esophagus.

ACKNOWLEDGMENTS

We would like to show our gratitude to the GPX medical team for the support throughout the experiment and Jonas Svensson at the Department of Medical Radiation Physics

for providing CT-images. We would also want to acknowledge Marcus Larsson, Sune Svanberg and Katarina Svanberg for valuable and fruitful discussions. This work was financially supported in part by the European Community (EUREKA EUROSTARS) NEOLUNG project (E! 9833 Neo-Lung), the LASERLAB-EUROPE (EUH2020 654148) JRA project BIOAPP and Departments of Pediatrics and Physics, Lund University, Lund, Sweden.

ORCID

Jim Larsson  <https://orcid.org/0000-0002-6213-240X>

REFERENCES

- [1] A. H. Jobe, *Am. J. Perinatol.* **2016**, *33*, 1076.
- [2] V. Fellman, L. Hellström-Westas, M. Norman, M. Westgren, K. Källén, H. Lagercrantz, K. Marsál, F. Serenius, M. Wennergren, E Group, *Obstetric Anesthesia Digest.* **2010**, *30*, 22.
- [3] P. Thunqvist, E. Tufvesson, L. Bjermer, A. Winberg, V. Fellman, M. Domellöf, E. Melén, M. Norman, J. Hallberg, *Pediatr. Pulmonol.* **2018**, *53*, 64.
- [4] S. Don, *Pediatr Radiol* **2004**, *34*, S167.
- [5] E. J. Hall, *Pediatr Radiol* **2002**, *32*, 700.
- [6] M. Miedema, F. H. de Jongh, I. Frerichs, M. B. van Veenendaal, A. H. van Kaam, *Am. J. Respir. Crit. Care Med.* **2011**, *184*, 100.
- [7] I. Chatziioannidis, T. Samaras, N. Nikolaidis, *Hippokratia* **2011**, *15*, 211.
- [8] H.-Y. Liang, X.-W. Liang, Z.-Y. Chen, X.-H. Tan, H.-H. Yang, J.-Y. Liao, K. Cai, J.-S. Yu *Quantitative Imaging in Medicine and Surgery*. Hong Kong, China: AME publications; **2018**.
- [9] E. K. Svanberg, P. Lundin, M. Larsson, J. Akesson, K. Svanberg, S. Svanberg, S. Andersson-Engels, V. Fellman, *Pediatr Res* **2016**, *79*, 621–628.
- [10] S. Svanberg, *Laser Photonics Rev* **2013**, *7*, 779.
- [11] T. Ligor, M. Ligor, A. Amann, C. Ager, M. Bachler, A. Dzien, B. Buszewski, *J. Breath Res.* **2008**, *2*, 046006.
- [12] P. Liao, J. Larsson, E. K. Svanberg, P. Lundin, J. Swartling, M. L. Xu, J. Bood, S. Andersson-Engels, *J Biophotonics* **2018**, *11*, e201800023.
- [13] J. Larsson, P. Liao, P. Lundin, E. Krite Svanberg, J. Swartling, M. Lewander Xu, J. Bood, S. Andersson-Engels, *J. Biophotonics* **2018**, *11*, e201700097.
- [14] Krite Svanberg E, Svanberg S. *Equipment and method for internal laser illumination for medical gas analysis*. Swedish Patent Application No 1500335-3. 2015.
- [15] Svanberg S, Krite Svanberg E, Larsson M. *System and method for laser based internal analysis of gases in a body*. Extended PCT application No: PCT/EP2016/069549.
- [16] Krite Svanberg E. Non-invasive optical monitoring of free and bound oxygen in human. [PhD thesis] Lund University; 2016.
- [17] H. Yonis, L. Crognier, J.-M. Conil, I. Serres, A. Rouget, M. Virtos, P. Cougot, V. Minville, O. Fourcade, B. Georges, *BMC Anesthesiol.* **2015**, *15*, 117.
- [18] Neo-Lung | EUROSTARS. <https://www.eurostars-eureka.eu/project/id/9833>. Accessed August 13, 2018.

- [19] S. Pålsson, L. Gustafsson, N. Bendsoe, M. Soto Thompson, S. Andersson-Engels, K. Svanberg, *Br J Dermatol.* **2003**, *148*, 1179.
- [20] D. Khoptyar, A. A. Subash, S. Johansson, M. Saleem, A. Sparén, J. Johansson, S. Andersson-Engels, *Opt. Express* **2013**, *21*, 20941.

How to cite this article: Larsson J, Leander D, Lewander Xu M, Fellman V, Bood J, Krite Svanberg E. Comparison of dermal vs internal light administration in human lungs using the TDLAS-GASMAS technique—Phantom studies. *J. Biophotonics*. 2019;e201800350. <https://doi.org/10.1002/jbio.201800350>